A highly robust and reusable polyimide-supported nanosilver catalyst for the reduction of 4-nitrophenol

Jun Li, Ya Wang, Mingyu Wang, Lisi Wang, and Hengfeng Li[a)]
Department of Materials Chemistry, School of Materials and Engineering, Central South University, Changsha, Hunan 410083, China

(Received 18 March 2015; accepted 7 August 2015)

A simple and efficient method for in situ preparation of highly stable polyimide (PI)-supported silver nanoparticles (AgNPs) was proposed. This process achieves excellent dispersion and high stability of AgNPs in the PI matrix. The formation of AgNPs in PI and the morphology evolution of PI/Ag nanocomposites were characterized by x-ray diffraction, transmission electron microscopy, Fourier transform infrared spectroscopy (FT-IR), and x-ray photoelectron spectra studies. The catalytic properties of these PI-supported AgNPs were investigated by monitoring the reduction of 4-nitrophenol by excess $NaBH_4$ in water. The catalytic reaction was observed to have a pseudo first-order rate constant of 0.567 min^{-1} (9.45×10^{-3} s^{-1}), which is comparable to other heterogeneous silver catalysts reported in the literature. Notably, the PI-supported AgNPs retained their relatively high catalytic activity over seven recycles with almost no leaching of catalytic species in the reaction solution. Moreover, the catalytic activity of the catalyst is still quite appreciable even after a six-month shelf-storage under room temperature.

I. INTRODUCTION

Recently, metal nanoparticles have attracted intensive attention in various areas, such as catalysis, optics, electromagnetics or plasmonics, antibacterials, etc.[1–6] The interest in these nanoparticles stems from their unique characteristics as compared to their bulk counterparts. For example, it has been both experimentally and industrially demonstrated that noble metallic nanoparticles perform better in catalysis because of their high chemical activity and specificity of interaction.[1,2] Among them, silver is the most attractive in terms of its much lower cost, and silver nanoparticles (AgNPs) are well known to be efficient catalysts for the selective oxidation of olefins and the reduction of many organic dyes and nitroaromatic compounds.[2,7–10] However, in most cases, the performance of the AgNPs degrades over time as a result of agglomeration and leaking during the fabrication and application processes. In this regard, AgNPs have often been immobilized onto various supports, including inorganic, organic, and polymeric materials.[7,11–14]

Since Merrifield[15] first reported the concept of solid-phase peptide synthesis with heterogeneous chloromethylated polystyrene half a century ago, many soluble or insoluble polymers have been widely implemented in organic synthesis and product isolation.[16–18] Although soluble polymer- or dendrimer-aided catalysis has received more attention in the academic community due to its huge activity, which is almost comparable to homogeneous catalysis, the relatively low rates of recovery and reuse of these labile catalysts are still urgent issues from an industrial perspective.[19–21] In contrast, the use of functional resins (i.e., insoluble polymers) as supports for metal nanoparticles is more favorable: they preserve a relatively high activity, provide for easy separation of the catalyst, and simplify the methods for recycling of the catalyst.[21,22]

Polyimide (PI) is a well-known high performance polymer, which possesses excellent thermal stability, robust physico-mechanical properties, and chemical resistance.[23] These characteristics allow PI to be widely used in high-temperature plastics, adhesives, microelectronics, dielectrics, optics, permeation, sensors, and memory devices, among others.[23–29] There are also some reports on the immobilization of homogeneous complex catalysts on functional PI.[30–32] For example, Ahn et al. developed a series of PI-supported Mo(VI) and Pt(II) complexes and found them to be effective catalysts in various oxidation reactions on both a laboratory and a technical scale; the supported Mo catalyst was highly active and could be recycled 10 times with no detectable loss.[30] To our surprise, however, very few studies concerning PI as a support for metal catalysts have been published to date, probably due to the facile migration and easy agglomeration of the metal nanoparticles during the conventional thermal treatment of PI synthesis, which results in the deteriorated catalytic activity and stability of the metal nanoparticles.[33,34] We have previously reported on an in situ preparation method of AgNPs in

Contributing Editor: Xiaobo Chen
[a)]Address all correspondence to this author.
e-mail: lihf@csu.edu.cn
DOI: 10.1557/jmr.2015.258

 © Materials Research Society 2015

https://doi.org/10.1557/jmr.2015.258 Published online by Cambridge University Press

a poly(amic acid) (PAA) solution and the possibility to prepare PI-encapsulated AgNPs via an in situ approach.[35] Inspired by the findings above, the objective of this article is to build an efficient all in situ strategy for the preparation of a PI-supported AgNPs catalyst, and for the reduction of 4-nitrophenol (4-NP) as a model reaction,[36] to examine its catalytic activity, recyclability, and shelf-storage stability.

II. EXPERIMENTAL SECTION

A. Materials

Silver nitrate ($AgNO_3$) was purchased from Hunan High Purity Chemical Reagent Company. 3,3′,4,4′-Benzophenonetetracarboxylic dianhydride (BTDA) was supplied by Beijing Multi Technology Co., Ltd. 4,4′-Diaminodiphenyl ether (ODA) was obtained from Shanghai Jiachen Chemical Co., Ltd. *N*,*N*-dimethylformamide (DMF), acetic anhydride, triethylamine, and anhydrous ethanol were purchased from Sinopharm Chemical Reagent Co., Ltd. All reagents were of analytical grade or better and used without further purification. 4-NPand $NaBH_4$ were purchased from Tianjin Kemiou Chemical Reagent Co., Ltd. Ultrapure water (18.25 MΩ cm, 25 °C) was used throughout the experiments.

B. In situ formation of AgNPs in a PAA solution

AgNPs were prepared according to the protocol reported in our previous study.[35] Briefly, 1.044 g of PAA was synthesized by reacting ODA (2 mmol) and BTDA (2.06 mmol) in DMF. The inherent viscosity of the resulting solution was 26.3 Pa s at 25 °C. The viscous PAA solution was then transferred to a 200 mL flask and diluted with DMF to obtain a 1% (m/m) PAA solution, followed by the direct addition of $AgNO_3$ (0.29 g). After the $AgNO_3$ was completely dissolved, the homogeneous solution was kept in a thermostat water bath at 80 °C for 10 h, without any further stirring. The color of the composite solution changed with time, from the pale yellow of the PAA matrix to a light reddish brown, and finally to a deep reddish brown, indicating the gradual formation of AgNPs in the medium. Different loadings of AgNPs in PAA solutions could be obtained by adding different amounts of $AgNO_3$, while keeping other conditions the same.

C. In situ embedment of AgNPs in the PI matrix

The loading of AgNPs into PI was achieved by the chemical imidization of PAA to PI and the concomitant embedment of AgNPs in PI. Under vigorous stirring, acetic anhydride (4 mL) and triethylamine (2 mL) were added dropwise to the AgNPs/PAA solution, as the imidization reaction progressed for 12 h, resulting in a dark brown suspension. The suspension was then poured slowly into 200 mL deionized water. The precipitate was collected by filtration and washed with ethanol several times to afford AgNPs/PI nanocomposites. The filtrate was treated with concentrated HCl or HNO_3 solutions to check for unreacted Ag^+ ions and AgNPs leached in the medium.

D. Catalytic studies

The catalytic properties of PI-supported AgNPs were investigated by using the reduction of 4-NP to 4-aminophenol (4-AP) by $NaBH_4$ as a model reaction. In a typical procedure, 4.5 mg of AgNPs/PI composite powder was added in the standard quartz cuvette with a 1-cm optical path length, followed by the addition of 3 mL of 10 mM $NaBH_4$ solution. Then 30 μL of 10 mM 4-NP was rapidly injected into the mixture by micropipette and the cuvette was shaken vigorously for mixing. The cuvette was then immediately placed in a UV–vis spectrophotometer to monitor the time-dependent absorption at 20 °C.

E. Analytical measurements

UV–vis spectra of the reaction solutions were measured by a UV–vis spectrophotometer (Shimadzu, model UV-2450, Tokyo, Japan) at a scanning speed of 1 nm/s. Transmission electron microscopy (TEM, model Tecnai G2 20 ST, Hillsboro, OR) of the samples was carried out by placing drops of solution or ethanol dispersion of composites on a carbon-coated copper grid and drying them at room temperature. The x-ray diffraction (XRD) patterns were recorded using a Japan Rigaku x-ray diffractometer (model D/max 2500/PC, Tokyo, Japan). The XRD samples were prepared by washing the composites with ethanol and dried in vacuum below 40 °C. Fourier transform infrared spectroscopy (FT-IR) investigations were performed using a Nicolet FT-IR instrument (model 6700, Waltham, MA) on the composite powder prepared by the same method as XRD. X-ray photoelectron spectra (XPS) were collected using a thermo scientific x-ray photoelectron spectrometer (model K-Alpha 1063, Waltham, MA), which is equipped with a microfocused monochromatic Al K_α x-ray source. The pressure in the analysis chamber was maintained at 10^{-9} mbar. Thermal gravimetric analysis (TGA) was performed on a simultaneous TGA/DSC (TA instruments, model SDT Q600, New Castle, DE) at a heating rate of 10 °C min^{-1} in air.

III. RESULTS AND DISCUSSION

A. Preparation and characterization of AgNPs/PI composites

A first attempt to in situ form AgNPs in a PI matrix by the thermal treatment method was made by curing AgNPs/PAA composite solutions at high temperature to obtain AgNPs/PI composites. However, no uniform dispersion but only irregular agglomerates of AgNPs in PI were obtained by this method. This may be due to the active migration/aggregation of AgNPs in PI and the

https://doi.org/10.1557/jmr.2015.258 Published online by Cambridge University Press

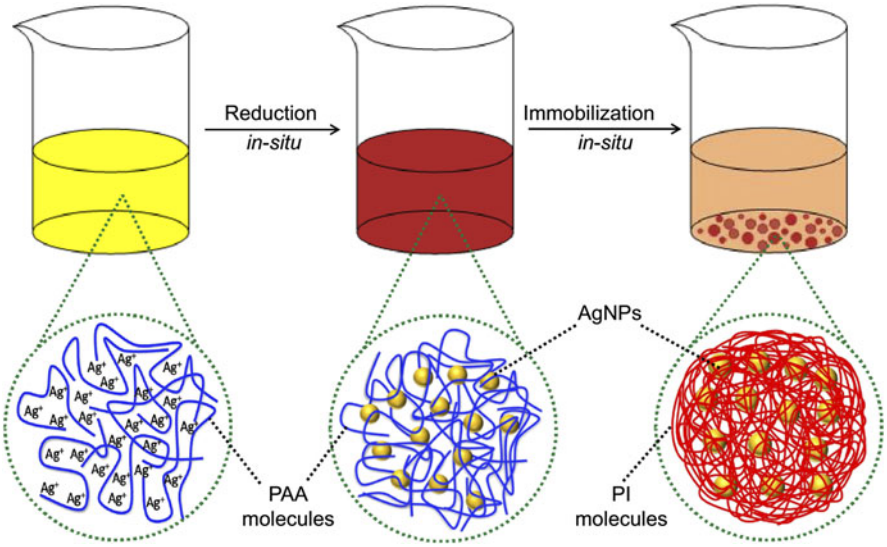


FIG. 1. Formation of AgNPs in PAA and PI through an all in situ approach.

silver-catalyzed oxidative degradation of PI matrix, driven by the heat.[37,38] On the other hand, as we previously reported, the strong cation-complexing ability and the considerable steric effect of PAA molecules make them a promising polymer protective agent for the preparation of AgNPs, and the resulting self-assembled coil-like structure provided a possibility to encapsulate AgNPs in PI via an in situ approach.[35,39] Therefore, in this article, a room-temperature chemical imidization method of PAA was adopted to prepare AgNPs/PI composites, to minimize the amount of AgNPs agglomeration.

The schematic diagram illustrating the in situ formation of AgNPs in PAA (denoted as AgNPs/PAA) and their in situ embedment in PI (denoted as AgNPs/PI) is shown in Fig. 1. In this approach, the in situ formation of AgNPs in PAA was first realized by a simple one-pot reduction of silver ions under the protection of PAA. Our previous work confirmed the initial formation of AgNPs in PAA, and no precipitation and absorbance changes were observed after 15-day storage at 10 °C.[35] The strong complexing power and coil-like structure of PAA molecules contribute to this homogeneous and highly stable dispersion of AgNPs in the PAA solution. To achieve a uniform immobilization of AgNPs in the final PI resin, the room-temperature chemical imidization reaction was then performed, in which PAA molecules were subject to rapid inter- or intracyclodehydration and thus formed AgNPs-embedded compact PI particulates. This mild fabrication process can effectively avoid migration and agglomeration of AgNPs in the PI, and AgNPs locked in these PI networks have excellent activity and stability in the catalytic applications.

We first consider the structural changes of matrixes during the processes. Figure 2 shows FT-IR spectra of AgNPs/PAA, AgNPs/PI, and cured AgNPs/PI. Before the

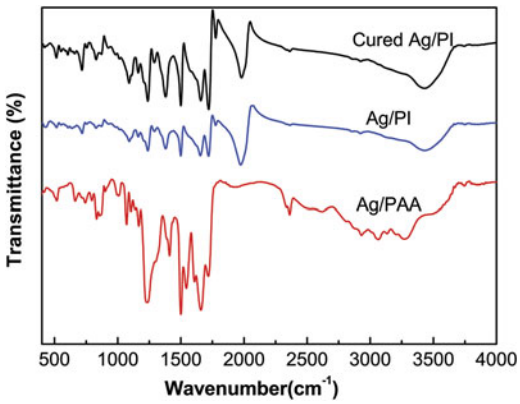


FIG. 2. FT-IR spectra of AgNPs/PAA, AgNPs/PI, and cured AgNPs/PI.

chemical imidization, the characteristic absorption bands of PAA molecules were easily recognized: the absorption band that occurs at 2370 and 1715 cm^{-1} was assigned to the vibration of carboxylic acid; the bands occurring at 1660, 1550, and 1410 cm^{-1} and the broad band from 3300 to 3000 cm^{-1} were assigned to the vibration of the amide groups.[40] It is worth noting that the capping effect can be attributed to the affinity of the carboxylic acid and amide moieties of PAA molecules for the AgNPs, which retards extensive agglomeration of the latter. Through the chemical imidization, most absorption of amide groups disappeared or was largely attenuated, while imide ring vibration increased, with associated bands at 1780, 1720, 1380, and 717 cm^{-1}, arising from asymmetric, symmetric carbonyl stretching vibrations, C–N axial stretching vibration and C=O bending vibration, respectively.[41] The results manifested the ring closure reaction caused by the chemical imidization. Upon annealing, the characteristic absorptions of imides further increased. In brief, PAA

https://doi.org/10.1557/jmr.2015.258 Published online by Cambridge University Press

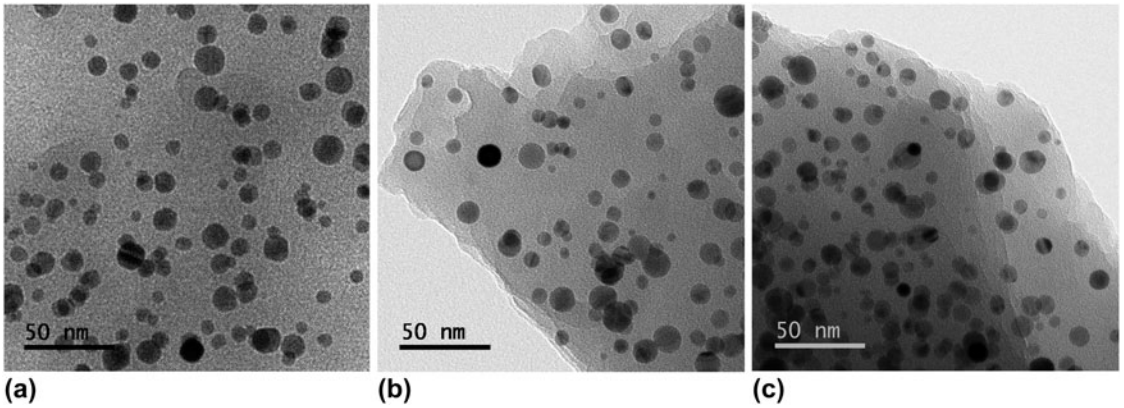


FIG. 3. (a) TEM image of AgNPs in PAA solutions; (b) TEM image of AgNPs/PI composites; (c) TEM image of AgNPs/PI composites after thermal treatment.

and PI molecules retain their integrity at each stage of processes, including the formation of AgNPs, chemical imidization, and thermal treatment.

To investigate the size distribution of AgNPs in the matrix and the morphology of nanocomposites, TEM studies were done. A typical TEM micrograph of drop-casting AgNPs/PAA solution is shown in Fig. 3(a). It is notable that spheroid AgNPs, with a uniform size distribution of 5–20 nm, are embedded in the homogeneous PAA medium, giving a direct proof for the good stability of AgNPs in PAA solutions. Therefore, PAA was believed to be effective in trapping small particles and rendering a uniform dispersion of AgNPs. Figure 3(b) displays a typical TEM image of AgNPs/PI nanocomposites prepared by the chemical imidization of AgNPs/PAA solution at room temperature. It is clear that AgNPs maintain the same nanoscale and uniform dispersion in the corresponding PI matrix. It is reasonable to image that the in situ formed semirigid PI molecular chains rapidly orientated, stacked, and immobilized AgNPs within, resulting in a strong mechanical interlocking interaction between them and the corresponding uniform dispersion of AgNPs in the final matrix.[37,42] It is also notable that our titration experiments detected no AgNPs in the filtrate, indicating that all Ag atoms were contained in PI matrix by this mechanical interlocking effect.

As shown in Fig. 3(c), with the aid of the thermal curing, PI molecules tended to optimize the orientation, shrink, and stack more compactly, leading to a rounded profile of composite powder and tighter interfaces between AgNPs and PI matrix. More importantly, TEM results indicate that ultrafine AgNPs were almost intact and their size and dispersion were excellently retained in the final composites. Therefore, our proposed two-step approach is shown to be effective in preparing the desired AgNPs/PI composites.

To further investigate the effect of chemical imidization and thermal curing processes, XRD tests were carried out on AgNPs/PAA, AgNPs/PI, and cured AgNPs/PI as shown in Fig. 4. Broad peaks at 20° and 19° are attributed to the amorphous phases of PAA and PI, respectively. Four well-defined peaks at 2θ = 38.2, 44.2, 64.5, and 77.4°, corresponding to the (111), (200), (220), and (311) planes of the face-centered cubic silver phase, respectively, could be readily detected. The broadening of these peaks confirms the existence of nanocrystals in the composites. The full width at half-maximum of the diffraction peaks of plane (111) is further used to estimate the average crystal sizes of AgNPs by applying the Scherrer's formula. The results are 12, 13, and 15 nm for AgNPs/PAA, AgNPs/PI, and cured AgNPs/PI, respectively, which are in good agreement with the TEM results. As such, the chemical imidization and the thermal curing did not affect the average crystallite sizes of the in situ formed AgNPs significantly, though the integrity of nanocrystals can be largely improved via the heat treatment. It is also worth mentioning that after performing chemical imidization, there are additional distinct diffraction peaks at about 31, 37, and 47°, which indicates some phase changes for the AgNPs/PI composites. Because these peaks gradually disappeared upon the thermal optimization, we speculate

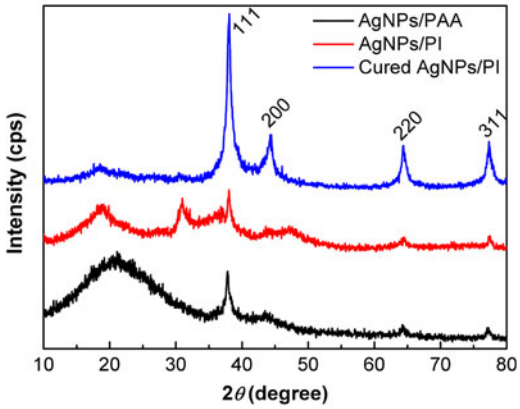


FIG. 4. XRD patterns of AgNPs/PAA, AgNPs/PI, and cured AgNPs/PI.

https://doi.org/10.1557/jmr.2015.258 Published online by Cambridge University Press

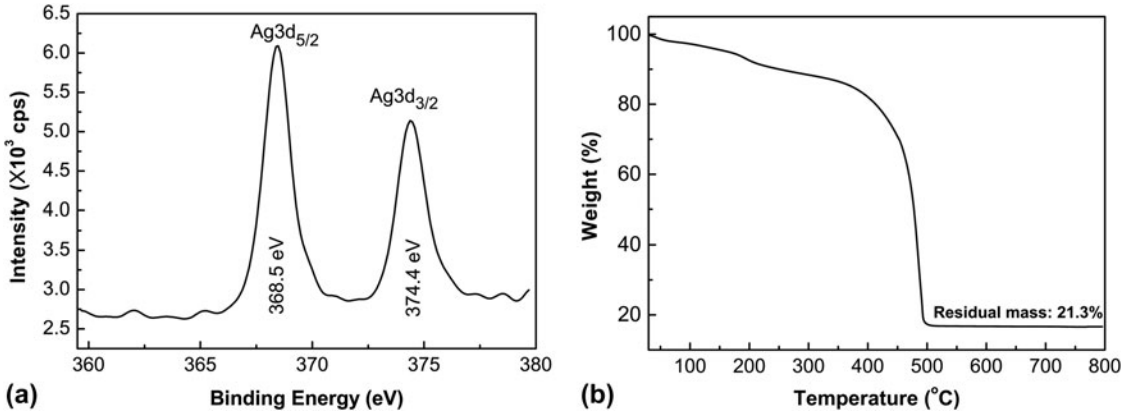


FIG. 5. (a) XPS Ag3*d* high-resolution spectra for AgNPs/PI composites; (b) TGA of the AgNPs/PI composites.

that they are closely related to the difficulty of orientation of sparsely solvated PI molecular chains during the rapid chemical cyclization.

The evidence of metallic silver within the PI resin was also confirmed by XPS in Fig. 5(a). Two specific peaks with binding energies of 374.4 and 368.5 eV are assigned to the Ag3$d_{3/2}$ and Ag3$d_{5/2}$ electrons of Ag^0, respectively. The surface elemental composition measurement indicates that the silver atomic concentration for the nanocomposites was 1.08 at.% (8.45 wt%), which was far less than that obtained from TGA (19.8 wt%) as shown in Fig. 5(b). In view of the fact that XPS can only detect elementary composition information at the materials' surface with a probing depth of less than 10 nm, we conclude that most AgNPs were embedded inside PI matrix. In other words, the migration and aggregation of AgNPs toward the surface of PI has been effectively avoided, which explains the uniform dispersion and the high stability of AgNPs.

B. Catalytic properties of PI-supported AgNPs

The catalytic reduction of 4-NP has recently been the most popular reaction to test the catalytic activity of metal nanoparticles because the reaction can be easily monitored in water by UV–vis spectroscopy. The absorption maximum of aqueous 4-NP was found to be at 317 nm (almost colorless), but when excess $NaBH_4$ was added, a red shift of the absorption peak to 400 nm appeared due to the formation of 4-nitrophenolate ions (yellow color). In the absence of any catalysts, the peak at 400 nm remained stable for hours. Figure 6 shows a typical time-dependent reduction of 4-NP in the presence of PI-supported AgNPs. It is clear that the peak at 400 nm decreased, with the concomitant increase of peak at 290 nm corresponding to the formation of 4-AP, and the yellow color of the solution faded to be colorless in less than 7 min. The isosbestic point at 316 nm also proved that the formation of 4-AP was as a result of the reduction of 4-NP catalyzed by PI-supported AgNPs.

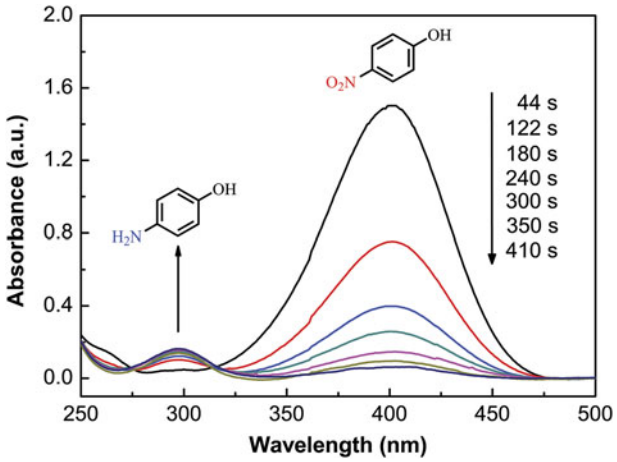


FIG. 6. UV–vis spectra of the solution of 4-NP catalyzed by PI-supported AgNPs as the function of time. Reaction conditions: (4-NP) = 0.1 mM; ($NaBH_4$) = 10 mM; catalyst = 4.5 mg.

When the initial concentration of 4-NP is very low and the concentration of $NaBH_4$ is in great excess compared with 4-NP, it is well accepted that the reduction reaction of 4-NP follows a pseudo first-order kinetic law:[8]

$$\frac{dc_t}{dt} = -k_{app}c_t \quad , \qquad (1)$$

where c_t refers to the concentration of 4-NP at time t, and k_{app} is the apparent rate constant. Based on Eq. (1) and Lambert–Beer's law, the decrease in the absorption at 400 nm can be used to determine the apparent rate constant k_{app} of catalytic reaction from the slope of the linear correlation of ln$A$ against time, where A is the absorption value of 4-NP. In this experiment, the amount of catalyst varied while keeping other parameters such as initial 4-NP and $NaBH_4$ concentrations constant, to study the effect of the amount of catalyst on the reaction rate. Table I lists the amount of nanocomposite used and corresponding Ag content

https://doi.org/10.1557/jmr.2015.258 Published online by Cambridge University Press

TABLE I. Amount of PI/AgNPs composite used in the catalytic studies and corresponding apparent reaction rate calculated from following kinetic analysis.

Test no.	Amount of PI/AgNPs composite (mg)	Corresponding Ag concentration (mg/L)[a]	Apparent reaction rate k_{app} (min^{-1})
1	1.0	66.1	0.02903
2	1.5	99.2	0.11596
3	2.3	152.0	0.20450
4	3.0	198.3	0.27261
5	3.8	251.2	0.35276
6	4.5	297.5	0.43355
7	5.2	343.7	0.56681

[a]The mass fraction of Ag in composite was calculated from the residual mass of composite in the TGA curve.

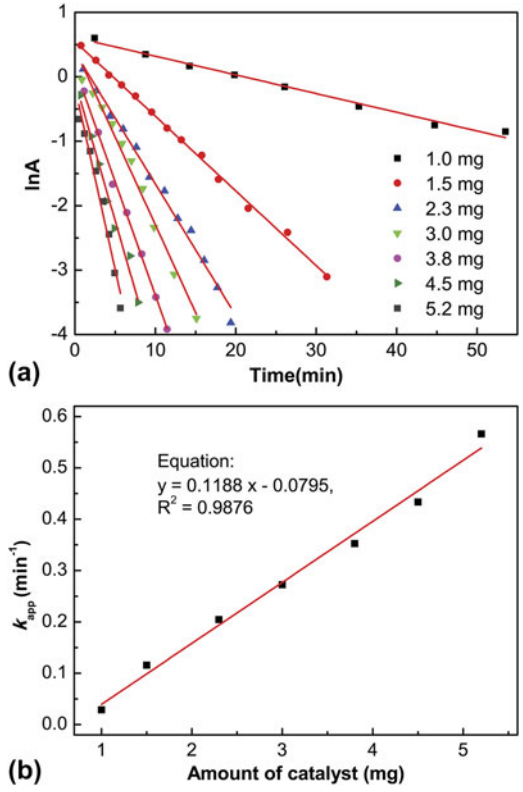


FIG. 7. Plots of (a) ln*A* versus time for different amounts of catalyst and (b) the apparent rate constant versus the amount of catalyst. Reaction conditions: (4-NP) = 0.1 mM; ($NaBH_4$) = 10 mM.

present in the final reaction medium. Plots of ln*A* versus time for different catalyst content are presented in Fig. 7(a).

Clearly, good linear relationships between ln*A* and the reaction time were obtained in all cases, and the reaction rate increases linearly with the increased concentration of catalyst as shown in Fig. 7(b). This is obviously due to an enlarged surface area of nanoparticles participating in the reaction. The maximum rate constant is 0.567 min^{-1} (9.45×10^{-3} s^{-1}), which is comparable to other supported Ag catalysts reported in the literature (Table II). Moreover, it must be noted that no significant induction period was observed in any of these catalytic reactions, regardless of how small the added concentration of AgNPs in the reaction was. The induction phenomenon is typical of heterogeneous catalysis and commonly related to the time required for the catalyst activation or surface restructuring, partially caused by the adsorbed substrate.[13,36] The high activity and "no-induction" phenomenon here is probably because the particular mechanical interlocking between the AgNPs and the PI matrix not only effectively prevents nanoparticles from aggregation and oxidation, but also makes the catalytically active sites on particles as accessible as possible.[8,49]

Beside the catalytic activity, the recovery and reusability of the catalyst are other important factors in the judgment of catalyst performance. Unfortunately, in many cases, either the recovery of the catalyst is inefficient (time-consuming and requiring complex handling), or the catalytic activity of nanocatalyst is deteriorative or even lost due to agglomeration effects or leaking of the nanoparticles.

To examine the reusability of the PI-supported AgNPs, we carried out a set of iterative catalytic experiments, where the dosage of the catalyst and other parameters were all kept nearly the same. The catalyst powder was separated from the mixture solution by decantation of the liquid through a filter membrane, followed by washing with deionized water and decantation of the liquid again. Finally, the catalyst was re-dispersed in the reaction solution for next cycle. As shown in Fig. 8, the catalytic activity of PI-supported AgNPs was retained quite well upon seven successive reaction cycles. The obvious

TABLE II. A comparison of catalytic activities of various supported AgNPs for the reduction of 4-NP.

Catalyst support	Temp. (°C)	(4-NP) (mM)	(BH_4^-) (mM)	(Ag) ($mg \cdot L^{-1}$)	k_{app} (s^{-1})	Refs.
Chitosan	23–24	0.1	10	273	2.68×10^{-3}	12
Carbon sphere	25	0.05	7.1	184	1.69×10^{-3}	43
Fe_3O_4@SiO_2	25	0.5	200	...	1.38×10^{-2}	44
Micro-SiO_2	22	0.1	10	107	3.56×10^{-3}	45
TiO_2	25	4.3	100	...	1.95×10^{-2}	46
Star-shaped copolymer	20	0.1	10	...	4.73×10^{-4}	47
Polypyrrole	25	0.11	300	750	1.10×10^{-3}	48
Polyimide	20	0.1	10	344	9.45×10^{-3}	This work

https://doi.org/10.1557/jmr.2015.258 Published online by Cambridge University Press

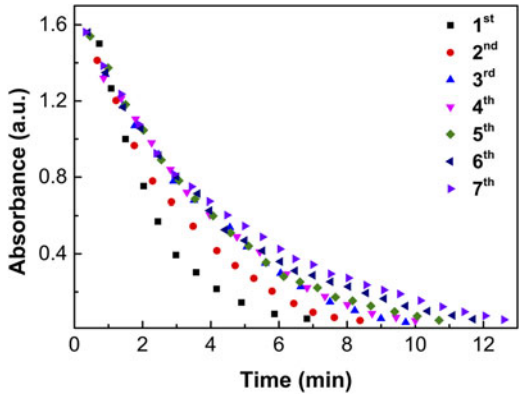


FIG. 8. Reusability of the PI-supported AgNPs catalyst. Reaction conditions: (4-NP) = 0.1 mM; ($NaBH_4$) = 10 mM; catalyst = 4.5 mg. The numbers in the top right corner indicate the cycle number in the catalytic experiments.

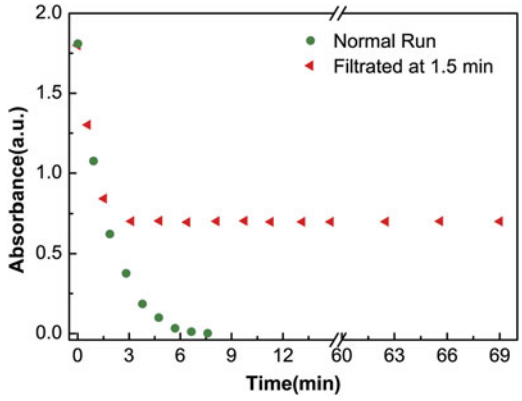


FIG. 9. Absorbance evolutions of 4-NP solutions in the normal run and after filtration of resin. Reaction conditions: (4-NP) = 0.1 mM; ($NaBH_4$) = 10 mM; catalyst = 4.5 mg.

additional time to deplete the 4-NP in the second and third cycles could be due to the loss of catalyst powder during the recovery handling, while once the loss of catalyst had reached saturation, the reaction maintained a relatively constant rate and could be completed within ~12 min. These results indicate that AgNPs embedded in PI resin were quite stable and stay active after repeated use. We speculate here that the encapsulation of AgNPs with semirigid PI molecules with the mechanical interlocking effect endows the AgNPs with a robust character, keeping them stable even under harsh reaction conditions. It is concluded that the PI-bound AgNPs are very effective for the catalytic reduction of 4-NP.

To test whether there was leaching of AgNPs from the PI matrix during the reaction, a filtration test was performed. As shown in Fig. 9, when the resin was separated from the reaction mixture by filtration after a 1.5 min reaction, the absorbance of filtrate remained completely constant for more than one hour. The inductively coupled plasma analysis indicated that no active silver species were leached

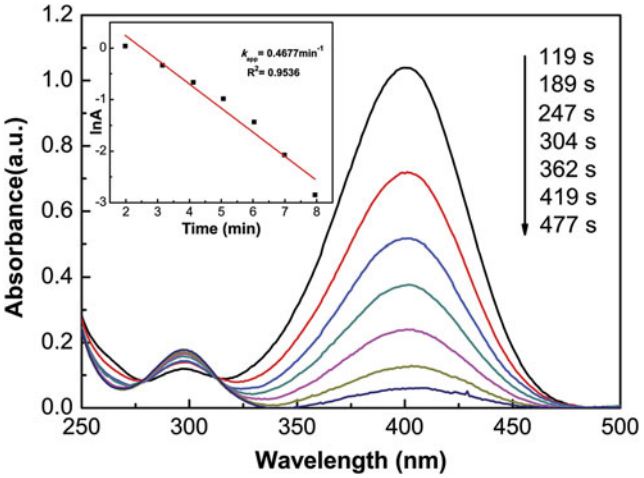


FIG. 10. Catalytic performance of the PI-supported AgNPs catalyst stored under ambient conditions for 6 mo. The inset shows the linear fitting of ln*A* at 400 nm versus reaction time. Reaction conditions: (4-NP) = 0.1 mM; ($NaBH_4$) = 10 mM; catalyst = 4.5 mg.

in the aqueous solution and further confirmed the high stability of AgNPs in the PI resin.

Considering that most noble metal catalysts suffer from limited shelf-storage stability or deactivation,[50,51] the storage stability of this nanocatalyst was also investigated by using the same batch of catalyst after six months of storage under room conditions. As shown in Fig. 10, the stock catalyst could still catalytically eliminate 4-NP completely within 8 min and thus maintains good to excellent catalytic activity as compared to freshly prepared sample (see Fig. 7). It is believed that the great chemical and mechanical properties of resin matrix and the especially interaction between the resin and AgNPs should be responsible for this outstanding stability. Therefore, PI is shown to be a promising candidate material for supporting nanoparticles catalysts.

IV. CONCLUSIONS

In summary, we have described a simple, efficient, and all in situ methods to prepare highly stable PI-supported AgNPs used as catalyst for the reduction of 4-NP. The homogeneous dispersion of AgNPs was in situ formed in PAA solutions, followed by the chemical imidization at ambient temperature, which resulted in excellent in situ dispersion and a high stability of AgNPs in the PI matrix. The PI-supported AgNPs had a good recyclable catalytic performance and excellent shelf-storage stability in the reduction of 4-NP, which may be attributed to the great chemical and mechanical properties of PI matrix and the mechanical interlocking effect between the resin and AgNPs. Given the above results, we conclude that PI-supported AgNPs are very effective for the catalytic reduction of 4-NP, and that PI is a promising candidate supporting material for metal nanoparticles.

https://doi.org/10.1557/jmr.2015.258 Published online by Cambridge University Press

Currently, we are conducting continuing studies on the fabrication of PI-supported various metal nanoparticles and their wider applications in catalysis.

ACKNOWLEDGMENTS

This work was supported by the Faculty Research Fund of Central South University (2013JSJJ002) and the Hunan Provincial Innovation Foundation for Graduate Students (CX2014B049).

REFERENCES

1. Y. Zhu, C.N. Lee, R.A. Kemp, N.S. Hosmane, and J.A. Maguire: Latest developments in the catalytic application of nanoscaled neutral group 8–10 metals. *Chem. - Asian J.* **3**, 650 (2008).
2. J.M. Campelo, D. Luna, R. Luque, J.M. Marinas, and A.A. Romero: Sustainable preparation of supported metal nanoparticles and their applications in catalysis. *ChemSusChem* **2**, 18 (2009).
3. N.J. Halas, S. Lal, W-S. Chang, S. Link, and P. Nordlander: Plasmons in strongly coupled metallic nanostructures. *Chem. Rev.* **111**, 3913 (2011).
4. P.K. Jain, X. Huang, I.H. El-Sayed, and M.A. El-Sayed: Noble metals on the nanoscale: optical and photothermal properties and some applications in imaging, sensing, biology, and medicine. *Acc. Chem. Res.* **41**, 1578 (2008).
5. J.A. Polo and A. Lakhtakia: Surface electromagnetic waves: A review. *Laser Photonics Rev.* **5**, 234 (2011).
6. C. Marambio-Jones and E.M. Hoek: A review of the antibacterial effects of silver nanomaterials and potential implications for human health and the environment. *J. Nanopart. Res.* **12**, 1531 (2010).
7. M. Zhu, C. Wang, D. Meng, and G. Diao: In situ synthesis of silver nanostructures on magnetic Fe_3O_4@C core–shell nanocomposites and their application in catalytic reduction reactions. *J. Mater. Chem. A* **1**, 2118 (2013).
8. S. Jana, S.K. Ghosh, S. Nath, S. Pande, S. Praharaj, S. Panigrahi, S. Basu, T. Endo, and T. Pal: Synthesis of silver nanoshell-coated cationic polystyrene beads: A solid phase catalyst for the reduction of 4-nitrophenol. *Appl. Catal., A* **313**, 41 (2006).
9. P. Christopher and S. Linic: Shape-and size-specific chemistry of Ag nanostructures in catalytic ethylene epoxidation. *ChemCatChem* **2**, 78 (2010).
10. D-H. Zhang, H-B. Li, G-D. Li, and J-S. Chen: Magnetically recyclable Ag-ferrite catalysts: General synthesis and support effects in the epoxidation of styrene. *Dalton Trans.* **47**, 10527 (2009).
11. P. Zhang, C. Shao, Z. Zhang, M. Zhang, J. Mu, Z. Guo, and Y. Liu: In situ assembly of well-dispersed Ag nanoparticles (AgNPs) on electrospun carbon nanofibers (CNFs) for catalytic reduction of 4-nitrophenol. *Nanoscale* **3**, 3357 (2011).
12. A. Murugadoss and A. Chattopadhyay: A'green'chitosan–silver nanoparticle composite as a heterogeneous as well as micro-heterogeneous catalyst. *Nanotechnology* **19**, 015603 (2008).
13. A.M. Signori, K.d.O. Santos, R. Eising, B.L. Albuquerque, F.C. Giacomelli, and J.B. Domingos: Formation of catalytic silver nanoparticles supported on branched polyethyleneimine derivatives. *Langmuir* **26**, 17772 (2010).
14. C. Wang, H. Yin, R. Chan, S. Peng, S. Dai, and S. Sun: One-pot synthesis of oleylamine coated AuAg alloy NPs and their catalysis for CO oxidation. *Chem. Mater.* **21**, 433 (2009).
15. R.B. Merrifield: Solid phase peptide synthesis. I. The synthesis of a tetrapeptide. *J. Am. Chem. Soc.* **85**, 2149 (1963).
16. D.E. Bergbreiter, J. Tian, and C. Hongfa: Using soluble polymer supports to facilitate homogeneous catalysis. *Chem. Rev.* **109**, 530 (2009).
17. J. Lu and P.H. Toy: Organic polymer supports for synthesis and for reagent and catalyst immobilization. *Chem. Rev.* **109**, 815 (2009).
18. B. Clapham, T.S. Reger, and K.D. Janda: Polymer-supported catalysis in synthetic organic chemistry. *Tetrahedron* **57**, 4637 (2001).
19. L. Wu, Y. Zhang, and Y-G. Ji: Homogeneous recyclable catalysts based on metal nanoparticles for organic synthesis. *Curr. Org. Chem.* **17**, 1288 (2013).
20. Y. Wang, Z. Xiao, and L. Wu: Metal-nanoparticles supported on solid as heterogeneous catalysts. *Curr. Org. Chem.* **17**, 1325 (2013).
21. P.G.N. Mertens, P. Vandezande, X. Ye, H. Poelman, D.E. De Vos, and I.F.J. Vankelecom: Membrane-occluded gold-palladium nanoclusters as heterogeneous catalysts for the selective oxidation of alcohols to carbonyl compounds. *Adv. Synth. Catal.* **350**, 1241 (2008).
22. B.M. Dioos, I.F. Vankelecom, and P.A. Jacobs: Aspects of immobilisation of catalysts on polymeric supports. *Adv. Synth. Catal.* **348**, 1413 (2006).
23. D-J. Liaw, K-L. Wang, Y-C. Huang, K-R. Lee, J-Y. Lai, and C-S. Ha: Advanced polyimide materials: Syntheses, physical properties and applications. *Prog. Polym. Sci.* **37**, 907 (2012).
24. A. Quaranta, S. Carturan, M. Bonafini, G. Maggioni, M. Tonezzer, G. Mattei, C. de Julian Fernandez, G. Della Mea, and P. Mazzoldi: Optical sensing to organic vapors of fluorinated polyimide nanocomposites containing silver nanoclusters. *Sens. Actuators, B* **118**, 418 (2006).
25. K. Vanherck, I. Vankelecom, and T. Verbiest: Improving fluxes of polyimide membranes containing gold nanoparticles by photothermal heating. *J. Membr. Sci.* **373**, 5 (2011).
26. S.R. Halper and R.M. Villahermosa: Cobalt-containing polyimides for moisture sensing and absorption. *ACS Appl. Mater. Interfaces* **1**, 1041 (2009).
27. S. Park, K. Kim, D.M. Kim, W. Kwon, J. Choi, and M. Ree: High temperature polyimide containing anthracene moiety and its structure, and interface, and nonvolatile memory behavior. *ACS Appl. Mater. Interfaces* **3**, 765 (2011).
28. C. Samyn, T. Verbiest, and A. Persoons: Second-order non-linear optical polymers. *Macromol. Rapid Commun.* **21**(1), 1–15 (2000).
29. Y. Matsumura, Y. Enomoto, T. Tsuruoka, K. Akamatsu, and H. Nawafune: Fabrication of copper damascene patterns on polyimide using direct metallization on trench templates generated by imprint lithography. *Langmuir* **26**, 12448 (2010).
30. J-H. Ahn, J-C. Kim, S-K. Ihm, C-G. Oh, and D.C. Sherrington: Epoxidation of olefins by molybdenum (VI) catalysts supported on functional polyimide particulates. *Ind. Eng. Chem. Res.* **44**, 8560 (2005).
31. R. Jin, Z. Bian, J. Li, M. Ding, and L. Gao: ZIF-8 crystal coatings on a polyimide substrate and their catalytic behaviours for the Knoevenagel reaction. *Dalton Trans.* **42**, 3936 (2013).
32. J-H. Ahn and D.C. Sherrington: Wacker oxidation of Oct-1-ene using a palladium (II) complex supported on cyano-functionalized polyimide beads. *Macromolecules* **29**, 4164 (1996).
33. J. Huang, X. Qian, J. Yin, Z. Zhu, and H. Xu: Preparation of soluble polyimide–silver nanocomposites by a convenient ultraviolet irradiation technique. *Mater. Chem. Phys.* **69**, 172 (2001).
34. Q. Zhang, D. Wu, S. Qi, Z. Wu, X. Yang, and R. Jin: Preparation of ultra-fine polyimide fibers containing silver nanoparticles via in situ technique. *Mater. Lett.* **61**, 4027 (2007).
35. J. Li, Y. Fang, G. He, and H. Li: Preparation and characterization of poly (amic acid)-stabilized silver nanoparticles. *J. Cent. South Univ.* **20**, 1475 (2013).
36. P. Herves, M. Pérez-Lorenzo, L.M. Liz-Marzán, J. Dzubiella, Y. Lu, and M. Ballauff: Catalysis by metallic nanoparticles in aqueous solution: Model reactions. *Chem. Soc. Rev.* **41**, 5577 (2012).

https://doi.org/10.1557/jmr.2015.258 Published online by Cambridge University Press

37. R.E. Southward and D.M. Stoakley: Reflective and electrically conductive surface silvered polyimide films and coatings prepared via unusual single-stage self-metallization techniques. *Prog. Org. Coat.* **41**, 99 (2001).
38. R.E. Southward and D.W. Thompson: Metal-polyimide nanocomposite films: Single-stage synthesis of silvered polyimide films prepared from silver (I) complexes and BPDA/4, 4'-ODA. *Chem. Mater.* **16**, 1277 (2004).
39. S. Qi, X. Shen, Z. Lin, G. Tian, D. Wu, and R. Jin: Synthesis of silver nanocubes with controlled size using water-soluble poly (amic acid) salt as the intermediate via a novel ion-exchange self-assembly technique. *Nanoscale* **5**, 12132 (2013).
40. N. Du, C. Wong, M. Feurstein, O.A. Sadik, C. Umbach, and B. Sammakia: Flexible poly (amic acid) conducting polymers: Effect of chemical composition on structural, electrochemical, and mechanical properties. *Langmuir* **26**, 14194 (2010).
41. X. Fang, Z. Wang, Z. Yang, L. Gao, Q. Li, and M. Ding: Novel polyimides derived from 2, 3, 3′, 4′-benzophenonetetracarboxylic dianhydride. *Polymer* **44**, 2641 (2003).
42. R.E. Southward, D.S. Thompson, D.W. Thompson, M.L. Caplan, and A.K. St.Clair: Synthesis of reflective polyimide films via in situ silver (I) reduction. *Chem. Mater.* **7**, 2171 (1995).
43. S. Tang, S. Vongehr, and X. Meng: Carbon spheres with controllable silver nanoparticle doping. *J. Phys. Chem. C* **114**, 977 (2009).
44. X. Du, J. He, J. Zhu, L. Sun, and S. An: Ag-deposited silica-coated Fe_3O_4 magnetic nanoparticles catalyzed reduction of p-nitrophenol. *Appl. Surf. Sci.* **258**, 2717 (2012).
45. M. Wang, D. Tian, P. Tian, and L. Yuan: Synthesis of micron-SiO_2@ nano-Ag particles and their catalytic performance in 4-nitrophenol reduction. *Appl. Surf. Sci.* **283**, 389 (2013).
46. S. Deshmukh, R. Dhokale, H. Yadav, S. Achary, and S. Delekar: Titania–supported silver nanoparticles: An efficient and reusable catalyst for reduction of 4-nitrophenol. *Appl. Surf. Sci.* **273**, 676 (2013).
47. X. Huang, Y. Xiao, W. Zhang, and M. Lang: In-situ formation of silver nanoparticles stabilized by amphiphilic star-shaped copolymer and their catalytic application. *Appl. Surf. Sci.* **258**, 2655 (2012).
48. M. Chang, T. Kim, H-W. Park, M. Kang, E. Reichmanis, and H. Yoon: Imparting chemical stability in nanoparticulate silver via a conjugated polymer casing approach. *ACS Appl. Mater. Interfaces* **4**, 4357 (2012).
49. N. Pradhan, A. Pal, and T. Pal: Silver nanoparticle catalyzed reduction of aromatic nitro compounds. *Colloids Surf., A* **196**, 247 (2002).
50. B.J. Hornstein and R.G. Finke: Transition-metal nanocluster catalysts: Scaled-up synthesis, characterization, storage conditions, stability, and catalytic activity before and after storage of polyoxoanion-and tetrabutylammonium-stabilized Ir (0) nanoclusters. *Chem. Mater.* **15**, 899 (2003).
51. C-W. Yen, M-L. Lin, A. Wang, S-A. Chen, J-M. Chen, and C-Y. Mou: CO oxidation catalyzed by Au–Ag bimetallic nanoparticles supported in mesoporous silica. *J. Phys. Chem. C* **113**, 17831 (2009).

https://doi.org/10.1557/jmr.2015.258 Published online by Cambridge University Press